THE JOURNAL OF PHYSICAL CHEMISTRY C

Article

pubs.acs.org/JPCC

Electric Double Layer Dynamics in Poly(ethylene oxide) $LiClO_4$ on Graphene Transistors

Hua-Min Li,[†,‡] Ke Xu,[†,§] Buchanan Bourdon,[†] Hao Lu,[†] Yu-Chuan Lin,[∥] Joshua A. Robinson,[∥] Alan C. Seabaugh,[†] and Susan K. Fullerton-Shirey*[,†,§]

[†]Department of Electrical Engineering, University of Notre Dame, Notre Dame, Indiana, United States

[‡]Department of Electrical Engineering, University at Buffalo, The State University of New York, Buffalo, New York, United States

[§]Department of Chemical and Petroleum Engineering, University of Pittsburgh, Pittsburgh, Pennsylvania, United States

[∥]Department of Materials Science and Engineering, Materials Research Institute, and The Center for 2D and Layered Materials, Pennsylvania State University, University Park, Pennsylvania, United States

Supporting Information

ABSTRACT: Formation of an electric double layer (EDL) is a powerful approach for exploring the electronic properties of two-dimensional (2D) materials because of the ultrahigh capacitance and induced charge in the 2D materials. In this work, epitaxial graphene Hall bar devices are gated with an EDL using a 1 μm thick solid polymer electrolyte, poly(ethylene oxide) and $LiClO_4$. In addition to carrier density and mobility, ion dynamics associated with the formation and dissipation of the EDL are measured as a function of temperature over a gate bias range of ±2 V. The room temperature EDL formation time (~1−100 s) is longer than the dissipation time (~10 ms). The EDL dissipation is modeled by a stretched exponential decay, and the temperature-dependent dissipation times are described by the Vogel−Fulcher−Tammann equation, reflecting the coupling between polymer and ion mobility. At low temperatures, approaching the glass transition temperature of the electrolyte, the dissipation times of both cations and anions exceed several hours, and both p- and n-type EDLs can persist in the absence of a gate bias. The measured temperature-dependent relaxation times qualitatively agree with COMSOL multiphysics simulations of time-dependent ion transport in the presence of an applied field.

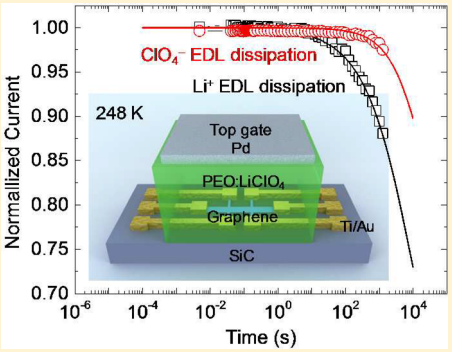

INTRODUCTION

By replacing a traditional gate dielectric with an electrolyte, new regimes of transport can be accessed in two-dimensional (2D) crystals. This approach exploits the creation of an electric double layer (EDL) that provides high capacitance density (~10 $\mu F/cm^2$) and field strengths exceeding 1 V/nm.[1−3] Compared to traditional doping strategies such as substitutional doping and molecular charge transfer doping, the formation of an EDL can provide an effective approach for controlling the conductivity of a semiconductor. In graphene, the EDL can induce charge carrier densities exceeding 10^{14} cm^{-2} for both electrons and holes.[4] EDLs are created using ionic liquids[1] and polymer electrolytes,[4] or a recently demonstrated monolayer, solid-state electrolyte.[5] EDL-induced ambipolar transport behavior has been demonstrated in 2D crystals, including MoS_2,[6,7] WSe_2,[8,9] WS_2,[10] $MoTe_2$,[11] and black phosphorus.[12] EDLs are now being broadly applied in the study of solid-state devices and phenomena including optoelectronics,[9] superconductivity,[13,14] and spintronics.[15]

While the dynamics of EDL formation and dissipation have been reported on ZnO for cationic double layers,[16,17] EDL dynamics on transistors based on 2D materials has not received much attention. A comprehensive and quantitative understanding of ion dynamics for both cations and anions is important to quantify the time scales required to establish and remove the EDL, which is critical for determining experimental procedures (e.g., equilibration time and sweep rate) and the operating speed of devices and circuits that may employ EDLs. In a solid polymer electrolyte, ion transport and polymer mobility are coupled and depend strongly on temperature.[18] This result has been demonstrated on ZnO FETs for both ionic liquids and polymer electrolytes.[16,17] In transistors, it is useful to form the EDL using applied biases and then lock the EDL in place by cooling below the glass transition temperature (T_g) of the electrolyte. This approach effectively arrests the mobility of the polymer and therefore the ions, making the EDL and the induced charge in the channel permanent. This ion-locking procedure is useful for doping transistor access regions and to create stable p−n junctions.[7,11] Compared to liquid electrolytes, one advantage of solid polymer electrolytes, such as those based on poly(ethylene oxide) (PEO), is their compatibility with electron beam lithography[19] and metal evaporation.[11]

Received: May 17, 2017
Revised: July 12, 2017
Published: July 14, 2017

DOI: 10.1021/acs.jpcc.7b04788
J. Phys. Chem. C 2017, 121, 16996−17004

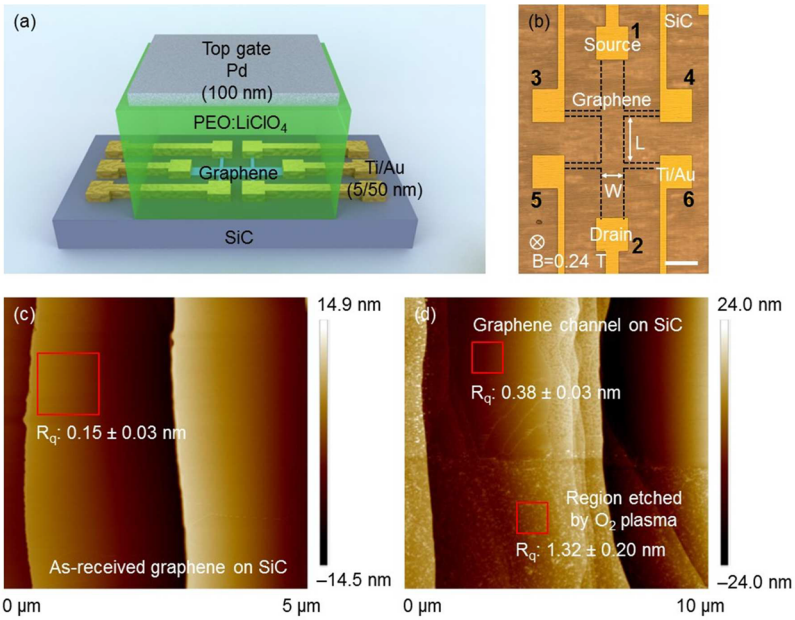

Figure 1. EDL-gated epitaxial graphene Hall bar. (a) Schematic of a graphene Hall bar on a SiC substrate with the polymer electrolyte shown over a small region of the device for clarity. (b) Optical image of the Hall bar; sufficient optical contrast does not exist between the graphene and the underlying SiC, and therefore the borders of the graphene are outlined by a dashed line. The length and width, L and W, are 160 and 80 μm, respectively. The scale bar is 100 μm. AFM scans of the graphene surface morphology on (c) an as-received sample (5 × 5 μm^2) and (d) after photolithography (10 × 10 μm^2). R_q is the root-mean-square value of the surface roughness calculated by averaging over 10, 1 × 1 μm^2 areas in each scan (examples of the 1 × 1 μm^2 areas are indicated by red boxes).

In this work, EDL dynamics are measured on Hall bar devices fabricated on epitaxial graphene and gated with a solid polymer electrolyte, PEO and $LiClO_4$. The temperature-dependent EDL formation and dissipation are investigated and compared for EDLs formed by both cations and anions. The results show that the EDL forms more slowly (~1−100 s at 298 K) than it dissipates (~10 ms at 298 K) for both types of ions. Within a few degrees above T_g, the EDL dissipates on the time scale of hours after removing a gate bias, demonstrating the long time scales over which the EDL can persist near the T_g.

EXPERIMENTAL METHODS

Materials and Device Fabrication. To prepare epitaxial graphene, 1 × 1 cm^2 substrates of 6H-SiC (II-VI Advanced Materials) were first cleaned via acetone, isopropyl alcohol, and deionized water and immersed in Piranha solution at 80 °C for 30 min, followed by deionized water rinse and an N_2 dry. Next, the samples were H-etched at 1500 °C in 700 Torr of H_2 (50 sccm)/Ar (450 sccm) for 30 min to remove polishing damage and to prepare a surface with atomically flat terraces. After H_2 etching, the system temperature was cooled to 850 °C and pumped and purged six times with ultrahigh purity N_2 to remove residual H_2 gas. The graphene was then prepared on the SiC substrate via solid-state decomposition, which was achieved by annealing at 1700 °C in a partial pressure of Ar (200 Torr, 500 sccm) for 20 min, driving the sublimation of Si atoms from the SiC substrate surface. The surface C atoms reorganize in this process into the hexagonal crystalline structure of graphene. On average, the graphene/SiC has 2 layers of graphene on the terrace and 4−7 layers on the step edges. The average terrace width and step height are 3−5 μm and 10−20 nm, respectively.[20]

Hall bar devices were patterned on the epitaxial graphene by photolithography. After precleaning by hot acetone, isopropyl alcohol, and deionized water, the epitaxial graphene was baked at 200 °C for 2 min to dehydrate the surface. A 400 nm thick undercut layer of polymethylglutarimide-SF9 (PMGI-SF9, MicroChem) was spin-coated, followed by a soft bake at 200 °C for 5 min. Then, a 1.2 μm thick, positive-tone photoresist MEGAPOSIT SPR700-1.2 (Rohm and Haas Electronic Materials) layer was spin-coated, followed by a soft bake at 95 °C for 1 min. After exposure, the sample was hard baked at 115 °C for 1 min and then developed in AZ917 MIF (Integrated Micro Materials), followed by a deionized water bath. To form the Hall bar geometry, an O_2 plasma etch was completed using a reactive ion etcher (RIE, PlasmaTherm 790 Series). An RF power of 150 W and dc voltage of 330 V were sufficient to remove the exposed graphene within 20 s at a pressure of 25 mTorr. Metal contacts, Ti (5 nm)/Au (50 nm), were deposited by electron beam evaporation. Lift-off was performed in hot acetone, followed by isopropyl alcohol, deionized water, AZ917 MIF, and deionized water bath, sequentially. The surface morphology of the graphene channel was characterized by atomic force microscopy (AFM, Bruker Dimension Icon).

The preparation and deposition of the polymer electrolyte were completed in an argon-filled glovebox where the concentrations of H_2O and O_2 were controlled to <0.1 ppm. PEO (molecular weight 95 000 g/mol, Polymer Standards Service) and $LiClO_4$ (99.9%, Sigma-Aldrich) were dissolved in anhydrous acetonitrile (Sigma-Aldrich) with a molar ratio of PEO ether oxygen to Li of 20:1 to make a 1 wt % solution. The graphene sample was coated with the PEO:$LiClO_4$ solution by drop-casting and annealed on a hot plate at 100 °C for 10 min to drive off the remaining solvent; both of these processes were completed in the Ar glovebox. After annealing, the PEO:$LiClO_4$

DOI: 10.1021/acs.jpcc.7b04788
J. Phys. Chem. C 2017, 121, 16996−17004

film thickness was measured as ~1 μm by scratching the polymer with tweezers down to the SiC substrate and taking multiple line scans using AFM. A 100 nm thick Pd top gate was deposited directly on the PEO:$LiClO_4$ film by electron beam evaporation through a shadow mask. A schematic of the device and an optical microscope image are shown in Figure 1a and b. It is important to note that the EDL dynamics presented in this article are expected to quantitatively change for varying electrolyte thicknesses, as highlighted by Lee et al., for a triblock copolymer electrolyte.[21] Specifically, the time constants will decrease with decreasing electrolyte thickness.

Electrical Characterization. Measurements were made on a Cascade Microtech Summit probe station filled with N_2 in a dark environment using an Agilent B1500 semiconductor parameter analyzer. The output and transfer characteristics of the EDL transistors were measured by setting contacts 1 and 2 as the source and drain, respectively; the source was common during the measurement. Top gate voltage, V_{TG}, was limited to a range of −2 to 2 V to avoid electrochemical reactions.

Hall Effect Measurement. Hall carrier density and mobility were obtained by a time-resolved Hall effect measurement configured on the probe station using a 1 × 1 cm^2 NdFeB permanent magnet (Amazing Magnets, Q152D) with a magnetic field (B) of 0.24 ± 0.01 T as measured by a Gaussmeter (LakeShore, 475 DSP). Top gate current (I_{TG}) was monitored during the measurement to detect charging and discharging. Both Hall voltage ($V_H = V_{21,56}$) and longitudinal voltage ($V_L = V_{21,64}$) were measured under a constant magnetic field with the graphene Hall bar device positioned on top of the permanent magnet. The Hall voltage was defined as the voltage difference between contacts 5 and 6 ($V_5 - V_6$) for a current flowing from contact 2 to 1, and longitudinal voltage was defined as the voltage difference between contacts 6 and 4 ($V_6 - V_4$) for the same current direction. Contact 1 was grounded; the current was applied to contact 2 (I_2) and varied from −5 to 5 μA to confirm the proportionality of Hall voltage to current and the expected dependence on current polarity. For the 2D geometry, the Hall coefficient per 2D layer thickness (R_H) is proportional to the graphene sheet carrier density (n_s) and can be written as $R_H = V_H/(I_2B) = 1/(qn_s)$ in cm^2/C, where B is the magnetic field and q is the elemental charge. The Hall mobility, $\mu_H = LI_2/(qn_sWV_L)$, and its dependence on n_s can also be extracted, where L and W are the length and width of the graphene channel, respectively. A positive sign for V_H and R_H indicates hole transport, and a negative sign indicates electron transport. To eliminate the effect of geometric asymmetry in the graphene Hall bar device, the Hall effect measurement was repeated at zero magnetic field (B = 0 T), and the Hall voltage at B = 0 T was subtracted from the measurement at B = 0.24 T.

Time-Resolved Measurement of EDL Formation and Dissipation. EDL formation and dissipation were measured by monitoring the drain current ($I_D = I_2$) as a function of time after the EDL-gate bias was applied or removed, respectively. During the entire measurement, the source was grounded, and a drain voltage ($V_D = V_2$) of 0.5 V was applied. All terminal voltages were set to 0 V for 10 min to establish equilibrium at room temperature before the start of the measurements. To drive cations (anions) to the surface of the graphene channel and induce n-type (p-type) doping, the voltage on a top gate to the PEO:$LiClO_4$ (V_{TG}) was set to 2 V (−2 V) for 10 min while monitoring the transition of I_D. The EDL formation time corresponded to the time required for I_D to increase from 10% to 90% of the signal. After 10 min of equilibration, V_{TG} was set to zero to dissipate the EDL. The dissipation time corresponded to the time required for I_D to decay from 90% to 10% of the signal. The same process was repeated three times for both V_{TG} = 2 and −2 V. In addition to the EDL induced by the top gate, it is noted that the ions can also migrate to form a p−i−n junction between source and drain, due to an electric field along the channel induced by the drain voltage. However, in our analysis, because $V_{TG} > V_{DS}$, the field perpendicular to the channel is assumed to dominate, and the drain-induced ion distribution along the channel is neglected.

Measurement of Temperature-Dependent EDL Dissipation. Following a similar procedure as described above for measuring the room-temperature dissipation time, the dissipation times of the Li^+ and ClO_4^- EDLs were monitored over a temperature (T) range of 298−248 K, stepped in −10 K increments. For this measurement, instead of cycling between positive and negative V_{TG}, one set of measurements was made at V_{TG} = 2 V over the entire temperature range for establishing the Li^+ EDL, and another set at V_{TG} = −2 V over the same range for establishing the ClO_4^- EDL. First, the EDL was formed at room temperature by applying a constant V_{TG} for 10 min with common source and drain. According to our measurements of EDL formation time (~1−100 s at 298 K), 10 min is sufficiently long to form the EDL. With V_{TG} applied, the sample was cooled to 288 K. After 10 min of thermal equilibration at this temperature, the top gate was set to 0 V, and the I_D transition was monitored for 20 min with the source at 0 V and V_D = 0.5 V. Next, the sample was returned to room temperature and equilibrated for 10 min to ensure a homogeneous distribution of ions for the next measurement. According to our measurement of EDL dissipation time (~10 ms at 298 K), 10 min is sufficient to removing any thermal hysteresis and reset the ions to equilibrium. The process was then repeated for the same V_{TG} at a temperature 10 K lower than the previous measurement. Last, the entire procedure was repeated for a V_{TG} with opposite polarity to determine the temperature-dependent dissipation times of both Li^+ and ClO_4^- EDLs.

RESULTS AND DISCUSSION

Because the EDL forms within <1 nm of the surface, it is important to start with a graphene surface that is free of photoresist; therefore, the surface morphology was characterized with AFM after photolithography and before electrolyte deposition. AFM scans of the as-received graphene and the postprocessed graphene are shown in Figure 1c and d. The average surface roughness (R_q) of the graphene after photolithography was 0.38 ± 0.03 nm, which is comparable with the as-received sample (0.15 ± 0.03 nm), suggesting that the surface is substantially free of photoresist residue and acceptable for polymer electrolyte deposition.

Schematics of EDL formation and the resulting n- and p-type doping of graphene are illustrated in Figure 2a−c. Assuming that the graphene is intrinsic, i.e., the Dirac point is located at V_{TG} = 0 V, both Li^+ and ClO_4^- are mobile and randomly distributed throughout the polymer electrolyte in the absence of a gate bias, as depicted in Figure 2a. When V_{TG} is positive, Li^+ cations are pushed to the surface of the graphene, forming an EDL with Debye length of ~1 nm and inducing n-type conductivity in the graphene, Figure 2b. Similarly, when V_{TG} is negative, ClO_4^- anions are pushed to the surface, inducing p-type conductivity, Figure 2c. Room temperature output characteristics are shown in Figure 2d at V_{TG} varying from

DOI: 10.1021/acs.jpcc.7b04788
J. Phys. Chem. C 2017, 121, 16996−17004

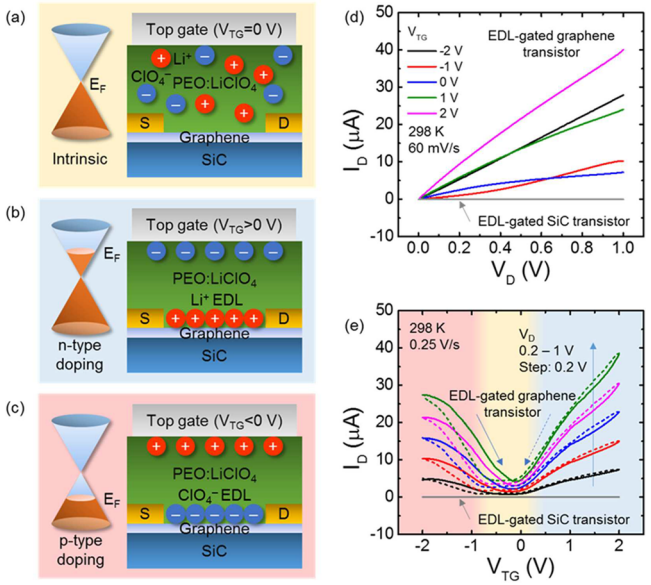

Figure 2. Common-source electrical characteristics of EDL-gated graphene Hall bar. (a) At V_{TG} = 0 V, ions are randomly distributed, and the graphene is intrinsic. (b) For V_{TG} > 0 V, the Li^+ EDL induces n-type doping. (c) For V_{TG} < 0 V, ClO_4^- EDL induces p-type doping. (d) Output and (e) transfer characteristics of the EDL-gated graphene transistor. In (e), the different background colors correspond to intrinsic, n-type, and p-type graphene as illustrated in (a)−(c). Solid and dashed lines denote forward sweep, from −2 to 2 V, and reverse sweep, from 2 to −2 V, of the top gate voltage, respectively. In (d) and (e), the gray lines are data for the EDL-gated SiC transistor (i.e., no graphene channel) with an identical device geometry under the same measurement conditions.

−2 to 2 V. The approximately linear relationship between I_D and V_D at low V_D (<0.2 V) indicates an Ohmic-like contact between the metal and the graphene and suggests that the ion doping effectively thins the Schottky barriers.[11] Room temperature transfer characteristics, shown in Figure 2e, indicate ambipolar carrier transport of the EDL-gated graphene with a hysteresis of ∼0.5 V at a sweep rate of 0.25 V/s. The low ionic conductivity of PEO:$LiClO_4$ (3×10^{-7} S/cm at 23 °C[22]) is a primary factor in the hysteretic response. Our previous work showed that the hysteresis can be reduced further by decreasing the sweep rate by 2 orders of magnitude to 1 mV/s.[11] The negative Dirac point voltage at around −0.5 V for both forward and reverse sweeps suggests that the graphene background doping is n-type. This is consistent with the presence of a carbon-rich buffer layer at the interface between graphene and SiC.[20] The measured I_{TG} ranges from 0.1 to 1 nA, which is approximately 3 orders of magnitude less than I_D at all V_{TG}. The bare SiC substrate surrounding the graphene channel can also be doped by the EDL. To quantify the contribution from the bare SiC substrate, control measurements were made on a device with the same geometry but for which the graphene channel was etched. The maximum drain current in the output and transfer characteristics of the bare SiC EDL transistor were ∼100 pA at 248 K, which is 4 orders of magnitude smaller than the drain currents in the graphene EDL transistor (∼1 μA) under the same measurement condition (see the Supporting Information). Therefore, the contribution from the SiC substrate to the drain current is negligible.

Time-resolved Hall effect measurements were made at room temperature to quantify the sheet carrier density and mobility of the EDL-gated epitaxial graphene. By applying a ramped I_2 and a pulsed V_{TG}, the transitions of I_{TG}, V_H, V_L, and R_H were monitored as functions of time (t) with data collected every 3 s and repeated three times, as shown in Figure 3a. Note that when V_{TG} = 0 V, the ions are free to respond to the applied V_{12} that is creating I_2, and this will result in alternating p−i−n and n−i−p doping profiles throughout the channel as a function of time. This inhomogeneous ion response gives rise to the features in V_H when V_{TG} = 0 V.

First we consider the changing spikes in I_{TG} in Figure 3a. A positive charging spike in I_{TG} is observed when V_{TG} = 1 V is applied at t = 10, 30, and 50 min, and a negative discharging spike is observed when V_{TG} is removed at t = 20, 40, and 60 min. Similarly, a negative charging spike and positive discharging spike were found for the case of the negative V_{TG}. The current spikes indicate that there are some shorter time processes related to EDL formation and dissipation at the metal top gate and at the graphene surface that cannot be captured by the instrument. In other words, some fraction of the EDL has formed and dissipated on a time scale faster than the resolution of the instrument. The magnitude of the current for the charging spikes at both positive and negative V_{TG} is larger than the corresponding discharging spikes, consistent with EDL formation occurring more slowly than dissipation (see Supporting Information). This conclusion is consistent with the dynamics of EDL formation and dissipation that are analyzed and discussed in greater detail below.

Next, we consider the Hall voltage response in Figure 3a. In thermodynamic equilibrium, the measured R_H and therefore n_s and μ_H should be independent of the current polarity and magnitude. Voltages V_H and V_L were measured and averaged at I_2 = 5 μA (at t = 15, 35, and 55 min) where the current is highest and Hall voltage is largest. At the maximum gate biases, n_s equals 5×10^{13} cm^{-2} for holes and -1×10^{13} cm^{-2} for electrons, as shown in Figure 3c. A previous report using the same electrolyte to gate graphene pushed the sheet carrier density to 10^{14} cm^{-2} using a larger gate voltage range of ±5 V.[4] As shown in Figure 3d, the maximum μ_H is approximately 480 $cm^2/(V\ s)$ near the Dirac point at room temperature, and μ_H decreases with increasing n_s due to carrier scattering.[23] The location of the Dirac points are different in the transfer characteristics compared to the time-resolved Hall effect measurement. Specifically, the locations are 0 V in the forward sweep and −0.7 V in the backward sweep in Figure 2e, compared to 0.25 V in Figure 3b−d. This difference is due to the different gate voltage sweep rates and directions of the two measurements. Compared to electron and hole mobility in graphene, ion mobility in a solid polymer electrolyte is small (1×10^{-9} $cm^2/(V\ s)$).[22] Therefore, carrier density modulation using an electrolyte depends strongly on the sweep rate and direction of the gate potential. In the transfer characteristics, the Dirac point is obtained by sweeping V_{TG} at 0.25 V/s. In contrast, for the time-resolved Hall effect measurements, a constant V_{TG} is applied for 10 min, so the sweep rate is effectively zero. Therefore, the Dirac point positions are different in these two measurements.

Time-resolved measurements of EDL formation and dissipation were made at room temperature to quantify the ion dynamics associated with ion drift and diffusion in response to an applied electric field. As shown in Figure 4a, with constant V_D = 0.5 V, a bipolar pulsing waveform was applied to the top gate to alternately set Li^+ and ClO_4^- EDLs on graphene; data were collected every 3 s. In agreement with the asymmetric

DOI: 10.1021/acs.jpcc.7b04788
J. Phys. Chem. C 2017, 121, 16996−17004

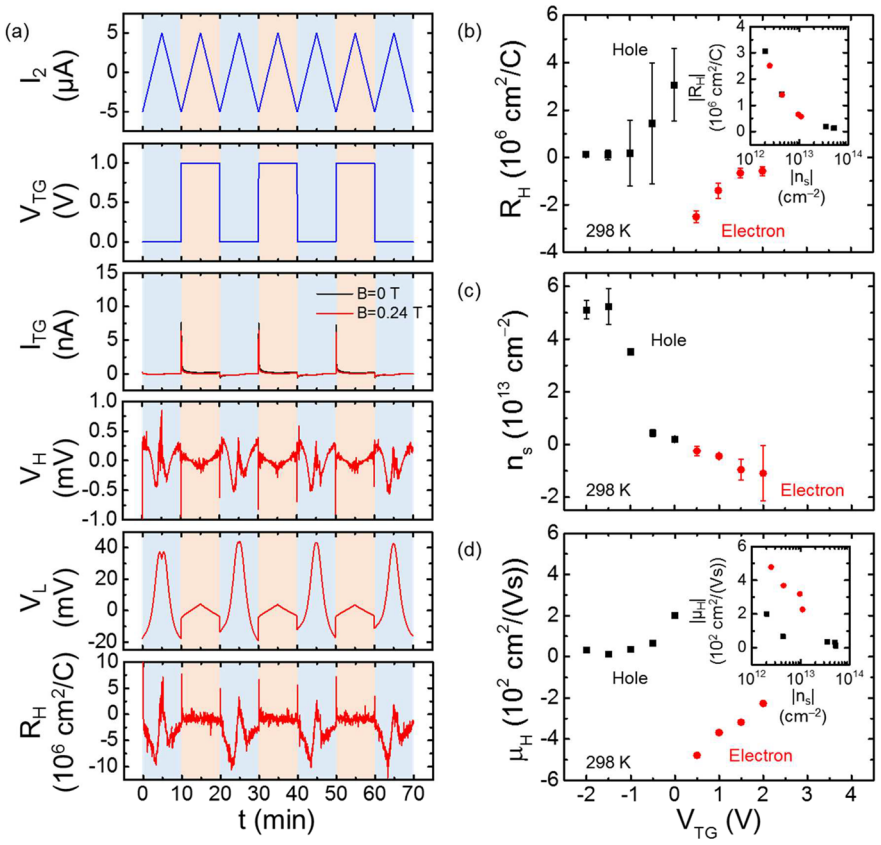

Figure 3. Time-resolved Hall effect measurements of EDL-gated graphene. (a) By applying a ramped I_2 with a V_{TG} pulse train, the I_{TG}, V_H, V_L, and R_H were measured as functions of time t. (b, c, d) R_H, n_S, and μ_H as functions of V_{TG}. Inset of (b) and (d), R_H and μ_H as functions of n_S for both holes and electrons.

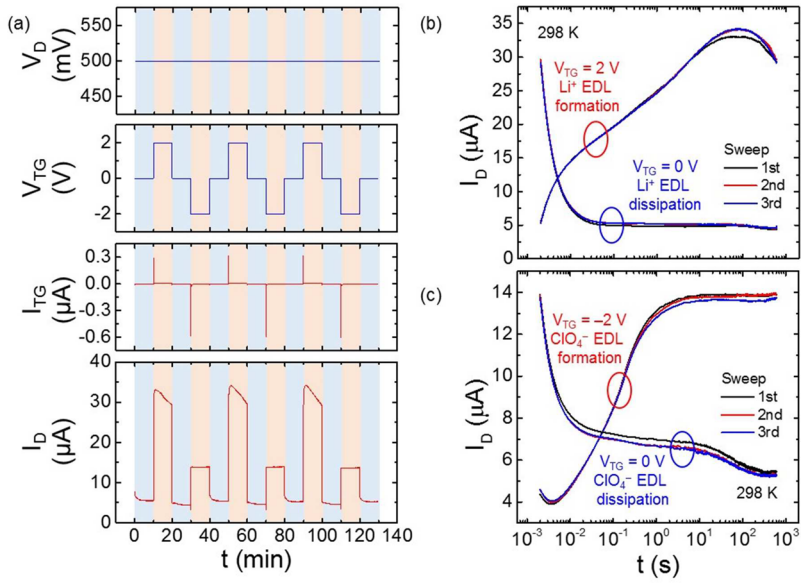

Figure 4. Characterization of EDL formation and dissipation at room temperature. (a) EDL formation and dissipation was measured by applying a V_{TG} pulse train at a fixed V_D = 0.5 V, and the transitions of I_{TG} and I_D were measured as functions of time t. Data were collected every 3 s. (b) Li^+ EDL formation (i.e., I_D increasing with t) and dissipation (i.e., I_D decreasing with t) as a function of time. (c) ClO_4^- EDL formation and dissipation as a function of time. Data in (b) and (c) were collected every 2 ms.

transfer characteristics, Figure 2e, the electron current at V_{TG} = 2 V is higher than the hole current at V_{TG} = −2 V. Displacement currents are again observed at the V_{TG} waveform transitions. Again higher displacement currents are observed at short times for EDL formation compared to dissipation; further, the displacement current for the zero to negative V_{TG} transition is greater than the zero to positive V_{TG} transition by approximately a factor of 2. The measurements for both of

DOI: 10.1021/acs.jpcc.7b04788
J. Phys. Chem. C 2017, 121, 16996−17004

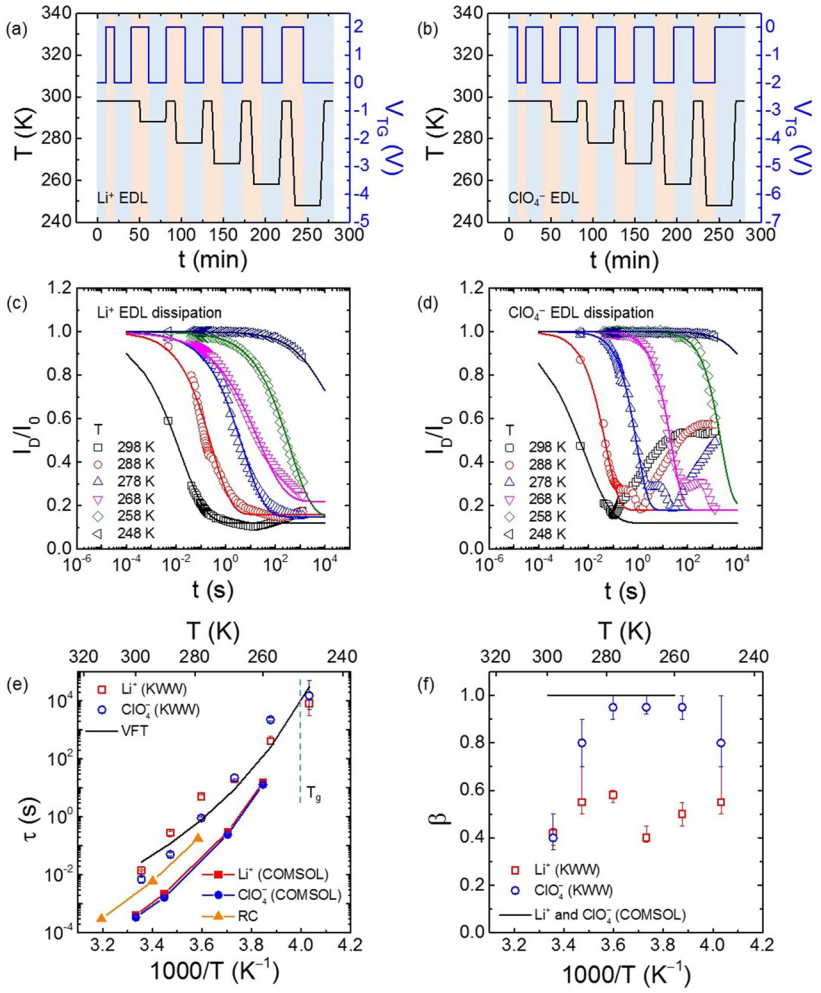

Figure 5. Temperature dependence of EDL dissipation. (a, b) T and V_{TG} profiles applied during the measurement for Li^+ EDL (V_{TG} = 2 V) and ClO_4^- EDL (V_{TG} = −2 V) dissipations. (c, d) I_D/I_0 as a function of t for Li^+ and ClO_4^- EDL dissipations. I_0 is the current at t = 0 s, defined as the time when V_{TG} changes from 2 (−2) to 0 V. The data in (c) and (d) are fit to the KWW equation, with the temperature-dependent τ and β plotted in (e) and (f). (e) τ as a function of 1000/T is fit to the VFT equation; also included are τ values from COMSOL multiphysics modeling for which the data is described by a single exponential decay, i.e., β = 1 in (f), and an estimate of the RC time constant. (e) β as a function of 1000/T. The error bars on the fits to the COMSOL data are within the size scale of the data points.

these currents is at the top gate electrode; therefore, the current results from EDL formation over short time scales at the top metal/electrolyte interface. The dynamics of this process will depend on anion and cation mobilities and the time-dependent electrostatic potential in the vicinity of the interface. Molecular modeling of these dynamics is needed to sort out the physics of this observation. We also note that the drain current, Figure 4a, is about 2 times higher for the $+V_{TG}$ bias condition which induces electron conduction than for the $-V_{TG}$ condition which induces hole conduction. This current ratio of electron/hole current is approximately proportional to $\mu_{Hn}\cdot n_{sn}/\mu_{Hp}\cdot n_{sp}$ = 1.6 at V_{TG} of ±2 V, where the subscript n and p denote the electron and hole, respectively.

For a more detailed look at the rise and decay of I_D corresponding to the formation and dissipation of the EDL, data were collected with a time resolution of 2 ms and are plotted in Figure 4b and c. The formation time of the Li^+ EDL is on the order of 100 s, whereas it is shorter for the ClO_4^- EDL, approximately 1 s. This is likely a consequence of the differing mobility between Li^+ and ClO_4^- in the polymer; the anion mobility is approximately three times larger than cation mobility.[24,25] Compared to the EDL formation, the dissipation time of both Li^+ and ClO_4^- EDLs is 3−4 orders of magnitude faster, approximately 10 ms. This result is expected when considering the contributions to the Nernst−Planck equation that describes species transport due to both a concentration gradient (∇c) and an electric field ($\nabla\phi$)

$$\frac{\partial c}{\partial t} = \nabla\cdot\left[D\nabla c + \frac{Dzq}{k_B T}c\nabla\phi\right] \quad (1)$$

where k_B is the Boltzmann constant, ϕ is the electrostatic potential, and c, D, and z are the volumetric concentration, diffusion coefficient, and valence (positive or negative charge state) of the ions, respectively. During the EDL formation, both contributions are significant, with diffusion due to a concentration gradient opposing drift. In contrast, the driving force during EDL dissipation is only the concentration gradient because the applied electric field is turned off (note that any contribution from the induced image charge in the graphene is neglected in the Nernst−Planck equation), leading to a process that completes more quickly than EDL formation.

As discussed in the Introduction, ion mobility through a polymer electrolyte is strongly coupled to polymer mobility;

DOI: 10.1021/acs.jpcc.7b04788
J. Phys. Chem. C 2017, 121, 16996−17004

therefore, the time constants associated with the formation and dissipation of the EDL will depend on polymer mobility.[18] The segmental relaxation time of a polymer follows a super-Arrhenius temperature dependence, where the mobility is arrested at temperatures below T_g of the polymer. Therefore, temperature-dependent ion dissipation measurements were performed at 248 K < T < 298 K, where the T_g of the polymer electrolyte is ∼250 K.[26] The temperature and bias profile are illustrated in Figure 5a and b for Li^+ EDL (V_{TG} = 2 V) and ClO_4^- EDL (V_{TG} = −2 V), respectively. The normalized current, I_D/I_0, versus t is shown in Figure 5c and d, where I_0 is the value of the current at t = 0 s when V_{TG} was changed from 2 (or −2) to 0 V. Therefore, the time scale over which the current decays will indicate how long the EDL persists at a given temperature. Consistent with the coupling between polymer and ion mobility, the EDL persists for longer times with decreasing temperature. It is noteworthy to highlight that the top gate is set to zero during the measurement of the EDL dissipation, and this is expected to accelerate the dissipation. If the terminal were floating instead, the induced image charge would delay the EDL relaxation dynamics.

The I_D/I_0 versus t data in Figure 5c and d can be fit to a stretched exponential equation, Kohlrausch−Williams−Watts (KWW), which is used to describe relaxation in polymers[27]

$$\frac{I_D}{I_0} = E + (1 - E)\exp\left[-\left(\frac{t}{\tau}\right)^{\beta}\right] \quad (2)$$

where E is the fraction of the decay that occurs outside the time window of the measurement, τ is the EDL dissipation time constant, and β is a stretching parameter which describes the distribution of dissipation times. In this case, I_D may not decay to zero when the EDL is fully dissipated, and therefore E will retain a nonzero value. When β = 1, the data can be described as a single exponential, where the EDL dissipates with a single time constant, τ; when β < 1, there exists a range of time constants during which the EDL dissipates. The dissipation times extracted from the KWW expression are provided in the Arrhenius plot as shown in Figure 5e. The extracted τ for both Li^+ and ClO_4^- ranges from ∼10 ms at room temperature to 10^4 s at T_g of ∼250 K, demonstrating the strong temperature dependence of the EDL dissipation and the long time scales over which the p- and n-type ion doping can persist, even in the absence of a gate bias. The temperature dependence of the dissipation times can be described by the Vogel−Fulcher−Tammann (VFT) equation as

$$\tau = \tau_0 \exp\left(\frac{\gamma T_{VF}}{T - T_{VF}}\right) \quad (3)$$

where τ_0 is the EDL relaxation time in the high-temperature limit, γ is a strength coefficient where larger γ indicates a stronger glassy material, and T_{VF} is the Vogel−Fulcher temperature or ideal glass temperature. Equation 3 is an empirical expression used to describe polymer mobility as a function of temperature. For the relaxation times shown in Figure 5e, τ_0, γ, and T_{VF} are 10^{-7} s, 5.8, and 205 K, respectively. The relaxation time in the high-temperature limit is several orders of magnitude larger than typically reported for solid polymer electrolytes.[26,28,29] However, the reported measurements were taken under AC bias conditions and therefore do not include polarization-induced Coulomb interaction between the ions in the polymer and the induced charge at the electrode surfaces. The Coulomb interaction would tend to increase the relaxation time of the EDL, accounting for the larger relaxation time measured in this study. Moreover, the speed of EDL formation and dissipation will decrease with decreasing electrolyte thickness.[21] In this study, the dynamics for only one electrolyte thickness (∼1 um) are reported. Both the magnitude and the temperature dependence of the relaxation data presented in Figure 5e show that the dissipation of the EDL is coupled to the dynamics of the polymer.

The room temperature relaxation time of ∼10 ms for both cations and anions is similar to the room temperature charging time of ∼7 ms reported for cations in the ionic liquid, DEME-TFSI, on a ZnO FET.[17] The authors used impedance spectroscopy to measure the frequency-dependent capacitance loss and extracted temperature-dependent polarization relaxation charging times. When comparing the time constants over the same temperature range for the two systems (i.e., room temperature to 250 K), the activation energy for the $(PEO)_{20}$:$LiClO_4$ electrolyte on graphene is ∼1700 meV whereas the DEME-TFSI electrolyte on ZnO is ∼300 meV. The nearly six times larger activation energy for the PEO-based electrolyte can be largely attributed to the difference in the T_g values between the two systems: 250 K for $(PEO)_{20}$:$LiClO_4$ and 182 K for DEME-TFSI. However, interaction strengths between the channel and the electrolyte would also be different for different combinations of polymers, ions, and channels.

In addition to the time constants extracted from the current measurements in Figure 5c and d, RC time constants were estimated using resistance values measured by impedance spectroscopy. Temperature-dependent impedance measurements were made in the frequency range of 40 Hz−110 MHz on the same polymer electrolyte used to gate the graphene devices; the experimental details and impedance data are provided in the Supporting Information. The sample geometry is a parallel plate capacitor where the electrolyte is hot pressed between two stainless steel electrodes to a diameter of 2.54 cm and a thickness of 100 μm. When the phase angle (θ) equals zero, the contribution to the impedance is purely resistive. The impedance values at θ = 0° equal 1.6×10^3, 2.6×10^4, and 7.3×10^5 Ω at 313, 294, and 279 K, respectively. Accounting for the device geometry, the resistivity values for the polymer electrolyte range from 10^5 to 10^8 Ω cm in this temperature window. Assuming C_{EDL} = 5 μF/cm^2 for an EDL-gated device with a top gate area of 0.1 cm^2 and an electrolyte thickness of 1 μm, the resistivity values are used to calculate RC time constants. As shown in Figure 5e, the time constants range from 0.3 ms at 313 K to 165 ms at 297 K and agree to within an order of magnitude with the dissipation times extracted from the I_D versus t data. It should be noted that the resistivity used to estimate the RC time constants was measured under a small ac voltage of 0.5 V, whereas a higher dc bias of 2 V was used to establish the EDL on the graphene Hall bars. While it is reasonable to expect that the resistivity will not depend on the voltage in the low-voltage limit (<0.5 V), it will likely depend on the voltage at 2 V. Specifically, the resistivity will likely increase with increasing bias, which would increase the dissipation time and bring the RC time constant estimate closer to the experimental result.

As discussed above, both Li^+ and ClO_4^- have similar EDL dissipation times; however, the distribution of times, described by β, is significantly different for cations versus anions, as shown in Figure 5f. As mentioned above, when β approaches 1, the distribution of dissipation times is narrow. Physically, this

DOI: 10.1021/acs.jpcc.7b04788
J. Phys. Chem. C 2017, 121, 16996−17004

can be interpreted as all the ions moving away from the interface with a similar time constant. The results shows $\beta_{ClO4-} > \beta_{Li+}$, meaning that the ClO_4^- ions dissipate from the surface with a narrower range of time constants compared to Li^+. It is possible that this difference is related to the intrinsic n-type doping of the graphene channel, Figure 2e. Even when V_{TG} is set to zero at t = 0 s, a small electric field due to the n-type doping could disrupt the Li^+ ions from moving away from the surface at the same time.

The EDL dissipation was modeled using COMSOL multiphysics. Ion diffusion in the presence of an applied electric field was modeled by coupling the Nernst−Planck and Poisson's equations as discussed in the Supporting Information. Diffusion coefficients for Li^+ and ClO_4^- were calculated based on ionic conductivity values from impedance measurements. Temperature-dependent dissipation times extracted from the COMSOL modeling are included in Figure 5e. Notice that the relaxation times from the modeling are approximately 1 order of magnitude smaller than the experimental values. This is reasonable because all the ions dissipate from the graphene surface at exactly the same time in the COMSOL model, giving rise to a perfect, single-exponential decay (i.e., β = 1) as shown in Figure 5f. In contrast, because the relaxation times in the experiments are distributed over a wide range (i.e., β < 1), the average relaxation time would be larger than predicted by theory. Moreover, the diffusion coefficients extracted from the impedance data and used in COMSOL are based on resistivity values measured in the low-voltage limit (i.e., 0.5 V). As mentioned above, the resistivity is expected to increase with increasing voltage, which may contribute to the offset between the measured dissipation time and the time predicted by theory.

It is noted that for the ClO_4^- EDL formation and dissipation, the measured current transition with time is not monotonic. For example, during the ClO_4^- EDL formation at room temperature, I_D decreases first and then starts to increase at $t \sim$ 4 ms (see Figure 4c). During the ClO_4^- EDL dissipation, I_D/I_0, after reaching the minimum, starts increasing at around 0.1, 1, and 20 s for T of 298, 288, and 278 K, respectively (see Figure 5d). These nonmonotonic transition with time can be understood by considering the intrinsic n-type doping of the graphene. As we observed in the transfer characteristics (see Figure 2e), the Dirac point is not at V_{TG} = 0 V but closer to −0.5 V; i.e., I_D is not at a minimum value at V_{TG} = 0 V. Therefore, when V_{TG} changes from 0 to −2 V for the ClO_4^- EDL formation, or vice versa for the ClO_4^- EDL dissipation, the current always decreases to the minimum and then starts to increase. This measurement can be further improved by changing the value of V_{TG} to $V_{TG} - V_{Dirac}$; thus, the graphene would be intrinsic at $V_{TG} - V_{Dirac}$. Also during the ClO_4^- EDL dissipation, Figure 5d, a plateau is found in the decreasing normalized current before reaching the minimum, and this reflects the plateau-shaped feature near the Dirac point in the reverse sweep of the transfer characteristic, Figure 2e. This feature only occurs in the reverse sweep when V_{TG} sweeps from −2 to 2 V, and it could be related to the charge transfer and trapping which have also been reported in other graphene transistors.[30]

In this work, the sample preparation and measurement condition were "dry;" i.e., the electrolyte was prepared and deposited inside a glovebox, and the devices were tested in a N_2 environment. However, the results will be significantly affected by exposure to water. Because the electrolytes are hygroscopic, and the water can act like a plasticizer that increases polymer and therefore ion mobility,[31] the EDL formation and dissipation times will decrease with the water exposure. The trade-off for faster EDL dynamics will be weakened EDL-gate control—an observation previously reported for a PEO electrolyte-gated device.[32]

CONCLUSIONS

Temperature-dependent dynamics of the EDL are measured on epitaxial graphene Hall bars gated by a solid polymer electrolyte. The temperature dependence of the EDL dissipation times agrees with modeling and verifies that the ion dynamics associated with the relaxation of the EDL are coupled to polymer mobility. The temperature dependence enables the EDL dissipation (or retention) time to be tuned by 6 orders of magnitude, from 10^{-2} to 10^4 s, in the temperature range of $T_g < T <$ 298 K for both p- and n-type doping. The retention times will be even longer at $T < T_g$, enabling the EDL to be "locked" into place even in the absence of a gate bias.

ASSOCIATED CONTENT

Supporting Information

The Supporting Information is available free of charge on the ACS Publications website at DOI: 10.1021/acs.jpcc.7b04788.

Impedance measurements to extract temperature-dependent diffusion coefficients (part 1); COMSOL modeling details (part 2); control experiments on EDL-gated SiC transistor (part 3); charging/discharging spikes (part 4); device-to-device performance variation (part 5) (PDF)

AUTHOR INFORMATION

Corresponding Author

*E-mail: Fullerton@pitt.edu.

ORCID

Ke Xu: 0000-0003-2692-1935

Joshua A. Robinson: 0000-0001-5427-5788

Susan K. Fullerton-Shirey: 0000-0003-2720-0400

Notes

The authors declare no competing financial interest.

ACKNOWLEDGMENTS

This work was supported in part by the Center for Low Energy Systems Technology (LEAST), one of six centers of STARnet, a Semiconductor Research Corporation program sponsored by MARCO and DARPA.

REFERENCES

(1) Ueno, K.; Shimotani, H.; Yuan, H.; Ye, J.; Kawasaki, M.; Iwasa, Y. Field-induced superconductivity in electric double layer transistors. *J. Phys. Soc. Jpn.* **2014**, *83*, 032001.

(2) Du, H.; Lin, X.; Xu, Z.; Chu, D. Electric double-layer transistors: A review of recent progress. *J. Mater. Sci.* **2015**, *50*, 5641−5673.

(3) Fujimoto, T.; Awaga, K. Electric-double-layer field-effect transistors with ionic liquids. *Phys. Chem. Chem. Phys.* **2013**, *15*, 8983−9006.

(4) Efetov, D. K.; Kim, P. Controlling electron-phonon interactions in graphene at ultrahigh carrier densities. *Phys. Rev. Lett.* **2010**, *105*, 256805.

(5) Xu, K.; Lu, H.; Kinder, E. W.; Seabaugh, A.; Fullerton-Shirey, S. K. Monolayer Solid-State Electrolyte for Electric Double Layer Gating of Graphene Field-Effect Transistors. *ACS Nano* **2017**, *11*, 5453−5464.

DOI: 10.1021/acs.jpcc.7b04788
J. Phys. Chem. C 2017, 121, 16996−17004

(6) Zhang, Y.; Ye, J.; Matsuhashi, Y.; Iwasa, Y. Ambipolar MoS_2 thin flake transistors. *Nano Lett.* **2012**, *12*, 1136−1140.
(7) Zhang, Y. J.; Ye, J. T.; Yomogida, Y.; Takenobu, T.; Iwasa, Y. Formation of a stable p−n junction in a liquid-gated MoS_2 ambipolar transistor. *Nano Lett.* **2013**, *13*, 3023−3028.
(8) Allain, A.; Kis, A. Electron and hole mobilities in single-layer WSe_2. *ACS Nano* **2014**, *8*, 7180−7185.
(9) Zhang, Y. J.; Oka, T.; Suzuki, R.; Ye, J. T.; Iwasa, Y. Electrically switchable chiral light-emitting transistor. *Science* **2014**, *344*, 725−728.
(10) Braga, D.; Gutiérrez Lezama, I. G.; Berger, H.; Morpurgo, A. F. Quantitative determination of the band gap of WS_2 with ambipolar ionic liquid-gated transistors. *Nano Lett.* **2012**, *12*, 5218−5223.
(11) Xu, H.; Fathipour, S.; Kinder, E. W.; Seabaugh, A. C.; Fullerton-Shirey, S. K. Reconfigurable ion gating of 2H-$MoTe_2$ field-effect transistors using poly(ethylene oxide)-$CsClO_4$ solid polymer electrolyte. *ACS Nano* **2015**, *9*, 4900−4910.
(12) Saito, Y.; Iwasa, Y. Ambipolar insulator-to-metal transition in black phosphorus by ionic-liquid gating. *ACS Nano* **2015**, *9*, 3192−3198.
(13) Ye, J. T.; Zhang, Y. J.; Akashi, R.; Bahramy, M. S.; Arita, R.; Iwasa, Y. Superconducting dome in a gate-tuned band insulator. *Science* **2012**, *338*, 1193−1196.
(14) Shi, W.; Ye, J.; Zhang, Y.; Suzuki, R.; Yoshida, M.; Miiyazak, J.; Inoue, N.; Saito, Y.; Iwasa, Y. Superconductivity series in transition metal dichalcogenides by ionic gating. *Sci. Rep.* **2015**, *5*, 12534.
(15) Yuan, H.; Wang, X.; Lian, B.; Zhang, H.; Fang, X.; Shen, B.; Xu, G.; Xu, Y.; Zhang, S.-C.; Hwang, H. Y.; Cui, Y. Generation and electric control of spin-valley-coupled circular photogalvanic current in WSe_2. *Nat. Nanotechnol.* **2014**, *9*, 851−857.
(16) Yuan, H.; Shimotani, H.; Tsukazaki, A.; Ohtomo, A.; Kawasaki, M.; Iwasa, Y. High-density carrier accumulation in ZnO field-effect transistors gated by electric double layers of ionic liquids. *Adv. Funct. Mater.* **2009**, *19*, 1046−1053.
(17) Yuan, H.; Shimotani, H.; Ye, J.; Yoon, S.; Aliah, H.; Tsukazaki, A.; Kawasaki, M.; Iwasa, Y. Electrostatic and electrochemical nature of liquid-gated electric-double-layer transistors based on oxide semiconductors. *J. Am. Chem. Soc.* **2010**, *132*, 18402−18407.
(18) Do, C.; Lunkenheimer, P.; Diddens, D.; Gotz, M.; Weiß, M.; Loidl, A.; Sun, X.-G.; Allgaier, J.; Ohl, M. Li^+ transport in poly(ethylene oxide) based electrolytes: Neutron scattering, dielectric spectroscoy, and molecular dynamics simulations. *Phys. Rev. Lett.* **2013**, *111*, 018301.
(19) Carrad, D. J.; Burke, A. M.; Lyttleton, R. W.; Joyce, H. J.; Tan, H. H.; Jagadish, C.; Storm, K.; Linke, H.; Samuelson, L.; Micolich, A. P. Electron-beam patterning of polymer electrolyte films to make multiple nanoscale gates for nanowire transistors. *Nano Lett.* **2014**, *14*, 94−100.
(20) Robinson, J. A.; Hollander, M.; LaBella, M.; Trumbull, K. A.; Cavalero, R.; Snyder, D. W. Epitaxial grahpene transistors: enhancing performance via hydrogen intercalation. *Nano Lett.* **2011**, *11*, 3875−3880.
(21) Lee, K. H.; Zhang, S.; Lodge, T. P.; Frisbie, C. D. Electrical impedance of spin-coatable ion gel films. *J. Phys. Chem. B* **2011**, *115*, 3315−3321.
(22) Do, N. S. T.; Schaetzl, D. M.; Dey, B.; Seabaugh, A. C.; Fullerton-Shirey, S. K. Influence of Fe_2O_3 nanofiller shape on the conductivity and thermal properties of solid polymer electrolytes: Nanorods versus nanospheres. *J. Phys. Chem. C* **2012**, *116*, 21216−21223.
(23) Zhu, W.; Perebeinos, V.; Freitag, M.; Avouris, P. Carrier scattering, mobilities, and electrostatic potential in monolayer, bilayer, and trilayer graphene. *Phys. Rev. B: Condens. Matter Mater. Phys.* **2009**, *80*, 235402.
(24) Gray, F. M. *Solid polymer electrolytes: Fundamentals and technological applications*; VCH: Weinheim, Germany, 1991.
(25) Wu, H.; Cummings, O. T.; Wick, C. D. Computational investigation on the effect of alumina hydration on lithium ion mobility in poly(ethylene oxide) $LiClO_4$ electrolytes. *J. Phys. Chem. B* **2012**, *116*, 14922−14932.
(26) Fullerton-Shirey, S. K.; Maranas, J. K. Effect of $LiClO_4$ on the structure and mobility of PEO-based solid polymer electrolytes. *Macromolecules* **2009**, *42*, 2142−2156.
(27) Williams, G.; Watts, D. C. Non-symmetrical dielectric relaxation behaviour arising from a simple empirical decay function. *Trans. Faraday Soc.* **1970**, *66*, 80−85.
(28) Wang, Y.; Fan, F.; Agapov, A. L.; Saito, T.; Yang, J.; Yu, X.; Hong, K.; Mays, J.; Sokolov, A. P. Examination of the fundamental relation between ionic transport and segmental and relaxation in polymer electrolytes. *Polymer* **2014**, *55*, 4067−4076.
(29) Mao, G.; Perea, R. F.; Howells, W. S.; Price, D. L.; Saboungi, L. Relaxation in polymer electrolytes on the nanosecond timescale. *Nature* **2000**, *405*, 163−165.
(30) Di Bartolomeo, A.; Giubileo, F.; Santandrea, S.; Romeo, F.; Citro, R.; Schroeder, T.; Lupina, G. Charge transfer and partial pinning at the contacts as the origin of a double dip in the transfer characteristics of graphene-based field-effect transistors. *Nanotechnology* **2011**, *22*, 275702.
(31) Fullerton-Shirey, S. K.; Ganapatibhotla, L. V. N. R.; Shi, W.; Maranas, J. K. Influence of thermal history and humidity on the ionic conductivity of nanoparticle-filled solid polymer electrolytes. *J. Polym. Sci., Part B: Polym. Phys.* **2011**, *49*, 1496−1505.
(32) Fathipour, S.; Xu, H.; Kinder, E.; Fullerton-Shirey, S.; Seabaugh, A. Investigation of aging and restoration of polyethylene-oxide cesium-perchlorate solid polymer electrolyte used for ion doping of a WSe_2 field-effect transistor. *72nd Device Research Conference (DRC)*, 2014; p 125.

DOI: 10.1021/acs.jpcc.7b04788
J. Phys. Chem. C 2017, 121, 16996−17004